

Focusing surface waves with an inhomogeneous metamaterial lens

Marco A. Escobar, Matthieu Berthomé, Changbao Ma, and Zhaowei Liu*

Department of Electrical and Computer Engineering, University of California,
San Diego, 9500 Gilman Drive, La Jolla, California 92093-0407, USA

*Corresponding author: zhaowei@ece.ucsd.edu

Received 3 August 2009; revised 20 October 2009; accepted 21 October 2009;
posted 26 October 2009 (Doc. ID 115149); published 10 November 2009

We propose a new type of surface wave lens that is made of a circular in-plane inhomogeneous metamaterial slab and numerically demonstrate its capability to focus surface waves at optical frequencies. This approach can achieve a smaller focal spot size than the previously demonstrated Ag plasmonic lens. The use of inhomogeneous metamaterials is to decrease the high losses that are usually associated with metamaterials that support large surface k vectors by reducing the propagation distance in high loss metamaterials. © 2009 Optical Society of America

OCIS codes: 240.6680, 240.6690, 250.5403, 160.3918.

1. Introduction

Surface plasmon polaritons (SPPs) are surface electromagnetic waves that are formed by collective oscillation of electrons at a metal–dielectric interface. Despite their inherent losses, SPPs can concentrate light into subwavelength scales and achieve optical field enhancements. For these reasons they have been used in microscopy, sensing, optical tweezers, nanolithography, waveguiding, and spectroscopy [1–4]. Structured metallic surfaces can be described by an effective dielectric function, and they support electromagnetic surface modes (SMs) [5] on the condition that the structure is on a scale much smaller than the working wavelength [6]. The ability to engineer materials to support SMs and modify their wavelengths at will opens opportunities to control and direct radiation on surfaces over a wide spectral range, incorporating optics into nanoscience and nanotechnology [1,7,8].

Confinement of SPPs at subwavelength spot sizes is desired to enhance resolution in some of the applications previously mentioned. Different approaches for focusing SPPs have been proposed, including

nanometric arrays of holes [9], tapered waveguides [10], V grooves [11], and plasmonic lenses [12]. For example, a plasmonic lens is a two-dimensional metallic element in which the energy transport lies completely on the surfaces of the lens. When an excitation light impinges the edges of a plasmonic lens, the diffracted light gains additional wave vectors (k vectors) along the surface, allowing a portion of the incident light to excite SPPs [13]. The slit can be modeled as a collection of SPP point sources that are located on the edge of the plasmonic lens. The wave vectors of the SPP sources are selected by the plasmonic lens material itself according to its own dispersion curve [14]. If normally incident free-space light is used for excitation, the in-plane wave vector will be completely produced by the light diffracted by the slit. The direction of the generated SPP wave vector, which determines the energy propagation direction, is perpendicular to the slit. For the particular case of an annular slit, the energy is guided toward the center of the ring [15,16]. The essence of the slit lies in its ability to generate high k vectors through diffraction. Other than the slit, an edge of the lens can also fulfill this duty, although its coupling efficiency might differ. For our study only the edge is used as the coupling mechanism.

0003-6935/10/070A18-05\$15.00/0
© 2010 Optical Society of America

At a given frequency, the wavelength of a non-radiative SPP (λ_{SPP}) is smaller than the free-space wavelength [14]. Therefore, the focal spot size of a plasmonic lens is below the free-space diffraction limit, which is approximately $\lambda_0/2$ [12]. The position of such focus can be tuned by changing the angle of incidence, as demonstrated in Ag plasmonic lenses [15].

We numerically demonstrate a new type of surface wave lens made of a circular metamaterial slab, which is inhomogeneous in the radial direction and composed of Ag nanowires in a dielectric matrix. In comparison with the Ag plasmonic lens, a smaller focal spot can be obtained with this surface wave lens and thus improved resolution can be achieved in the previously mentioned applications, because the metamaterial–air interface can be designed to have a SM wavelength smaller than the wavelength of the SPPs on the Ag–air interface. The SM existence conditions at an interface between an anisotropic material and air are analyzed in Section 2. Then, based on the analyzed SM existence conditions, appropriate metamaterials are designed in Section 3. The proposed surface wave lenses with smaller focal spots are demonstrated and discussed in Section 4. We give our conclusions in Section 5.

2. Conditions for the Existence of Surface Waves

To analyze the existing conditions for the SMs of an inhomogeneous metamaterial lens, we consider the surface of a nonmagnetic metamaterial (permeability $\mu = 1$) in air, as shown in Fig. 1. The material of the lens is considered to be a uniaxial crystal with two principal dielectric constants, ϵ_x and ϵ_z , in the x and z directions, respectively. Under this condition, only transverse magnetic (TM) surface modes are supported, and their dispersion relation in the boundary between air and anisotropic media is given by [17]

$$k_x^2 = \frac{\omega^2 \epsilon_z (1 - \epsilon_x)}{c^2 (1 - \epsilon_x \epsilon_z)}, \quad (1)$$

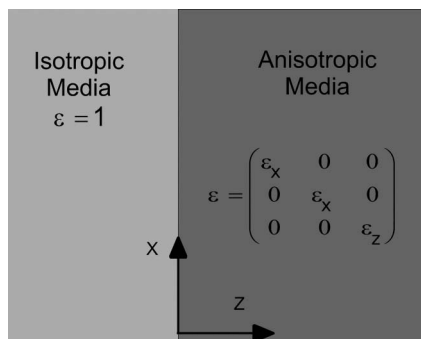


Fig. 1. (Color online) Diagram of the interface between air and an anisotropic medium. SMs propagate along the boundary surface of the two media, i.e., the x direction, and decay exponentially in the transverse direction, i.e., the z direction. The field maximum of SMs is at the interface, i.e., at $z = 0$.

where k_x is the wave vector of the SM in the propagation direction, ω is the angular frequency, and c is the speed of light in vacuum. A confined SM propagates along the boundary surface of two media and decays exponentially in the direction transverse to the propagation direction, attaining its maximum field at the interface. Thus k_x^2 in Eq. (1) must be positive. The attenuation constant in the isotropic medium is [17]

$$\alpha_1 = \frac{\omega}{c} \sqrt{\frac{(\epsilon_z - 1)}{1 - \epsilon_x \epsilon_z}}, \quad (2)$$

and the attenuation constant in the anisotropic medium is

$$\alpha_2 = -\alpha_1 \epsilon_x. \quad (3)$$

The real part of both attenuation constants also needs to be positive. These three conditions ensure the existence of SMs on an interface between an anisotropic nonmagnetic material and air.

The real (ϵ_x, ϵ_z) space can be divided into four quadrants, as shown in Fig. 2. Based on the conditions analyzed above, we can see that only quadrants II and III can sustain SMs. Quadrant II represents indefinite media [18]: ϵ_x and ϵ_z have different signs. And quadrant III represents metallike media: ϵ_x and ϵ_z are both negative. Moreover, in quadrants II and III, SMs exist only when $\epsilon_z > 1$ and $\epsilon_x \epsilon_z > 1$, which is shown as two separate areas, respectively. The material properties ϵ_x and ϵ_z are identical for isotropic metals, and thus they can be represented by a straight line in (ϵ_x, ϵ_z) space (see the gray line in Fig. 2). The metamaterial properties can be used to artificially tailor the (ϵ_x, ϵ_z) space and thus provide vast new opportunities to manipulate surface waves in comparison with natural isotropic metals. One specific

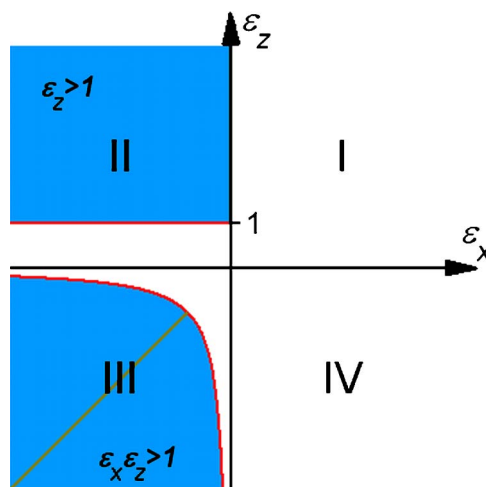


Fig. 2. (Color online) Existing conditions of SMs on the interface between an anisotropic and an isotropic medium. SMs exist only in quadrant II when $\epsilon_z > 1$ and in quadrant III when $\epsilon_x \epsilon_z > 1$. The gray line represents the values that an isotropic metal (i.e., Ag) can take.

example will be used to illustrate how the metamaterial is designed and utilized to control the surface waves in the following sections.

3. Metamaterial Modeling

Metamaterials offer electromagnetic properties that are difficult or impossible to achieve with natural materials. The metamaterial of a metallic nanowire array in a dielectric background can possess high anisotropy [19], which is useful to achieve surface wave manipulations. In addition, current developments in nanofabrication allow for the realization of well-aligned metallic nanowires with large aspect ratios in dielectric matrices [20–22]. As a result, we chose metallic nanowire arrays embedded in a dielectric host as a metamaterial example to design a surface wave lens.

The electromagnetic properties of metallic nanowire arrays have been investigated in the context of effective media theory, which allows metamaterials to be described with homogenized material parameters. The permittivities parallel and perpendicular to the wires are given by [23]

$$\varepsilon_{\parallel} = p\varepsilon_m + (1-p)\varepsilon_d, \quad (4)$$

$$\varepsilon_{\perp} = \varepsilon_d + \frac{p\varepsilon_d(\varepsilon_m - \varepsilon_d)}{\varepsilon_d + q(1-p)(\varepsilon_m - \varepsilon_d)}, \quad (5)$$

where ε_m is the permittivity of the metal, ε_d is the permittivity of the dielectric, q is the effective depolarization factor perpendicular to the nanowires (at the long wavelength limit of $q = 1/2$), and p is the volume filling ratio of metal.

As is shown above in Eqs. (4) and (5), the metal, dielectric, filling ratio, and working wavelength can be varied to design the desired material properties. For simplicity, we consider the metamaterial with nanowires that are perpendicular to the surface of the lens in such a way that $\varepsilon_{\perp} = \varepsilon_x$ and $\varepsilon_{\parallel} = \varepsilon_z$. Although not presented here, our simulations over different metals, including Ag, Au, and Al, and dielectric materials with a broad range of refractive index from 1.0 to 2.2, suggest that the combination of Ag and $n = 2.2$ is a good candidate for the surface wave lens in terms of relatively low loss and a favorable working wavelength.

We apply the effective medium theory to estimate our metamaterial properties. The Drude model $\varepsilon_m(\omega) = \varepsilon_{\infty} - \omega_p^2 / [\omega(\omega - i\gamma_c)]$ is used for the dispersion of Ag, with the high-frequency bulk permittivity $\varepsilon_{\infty} = 6.0$, the bulk plasmon frequency $\omega_p = 1.5 \times 10^{16}$ rad/s, and the collision frequency $\gamma_c = 7.73 \times 10^{13}$ Hz [23]. Using the SM existence conditions described above in Section 2, the wavelengths of the surface waves with respect to free-space wavelength λ_0 and the metal filling ratio are calculated to identify the regimes in which a shorter surface wave wavelength can be achieved. The calculated surface wave wavelengths on the air–metamaterial interface

(λ_{meta}) normalized with respect to the operating wavelengths (λ_0) and the SPP wavelengths on λ_{Ag} , as a function of λ_0 and the filling ratio are plotted in Figs. 3(a) and 3(b), respectively. Note that regions II and III in Fig. 3 correspond to regions II and III in Fig. 2, respectively. We see a plasmon-type behavior ($\lambda_{\text{meta}} < \lambda_0$) everywhere within the shaded area, as shown in Fig. 3(a), and there are areas in which $\lambda_{\text{meta}} < \lambda_{\text{Ag}}$, e.g., the lower parts in regions II and III in Fig. 3(b). These regions are of interest because smaller wavelengths lie in these regions and thus can be translated into a smaller focus in a plasmonic lens structure, although there could be high losses associated with these regions because of the SPP resonances.

Propagation length δ is the distance at which the field decays to $1/e$ and can be used as a measure of the losses. Figure 4 shows the ratio of the propagation length of the surface waves on the interfaces of Ag–air to metamaterial–air $\delta_{\text{Ag}}/\delta_{\text{meta}}$ as a function of the filling ratio at $\lambda_0 = 400$ nm. The solid curve is in region II and the dashed curve is in region III. It can be seen that as the filling ratio decreases, $\delta_{\text{Ag}}/\delta_{\text{meta}}$ increases and thus the loss increases. This conclusion offers a guideline for the design of a metamaterial surface wave lens. For example, in region III, if the single filling ratio of 0.6 is used in such a lens, the losses could be an order of magnitude higher than for Ag, although the wavelength of the SM could be very short (λ_{meta} is calculated to be 264 nm). So it is not feasible to design a metamaterial surface wave lens with low filling ratios in region III. In the following, we propose and numerically demonstrate a new surface wave lens using inhomogeneous metamaterials by varying the filling ratio from 0.6 to 0.9 in such a way that the propagation length in the lossiest material is reduced and a smaller focal spot is achieved.

4. Lens Design and Numerical Demonstration

The proposed surface wave lens is schematically shown in Fig. 5. It has a diameter of $6 \mu\text{m}$ and is composed of 20 homogeneous cylinders. Each cylinder is designed to have different effective permittivities by

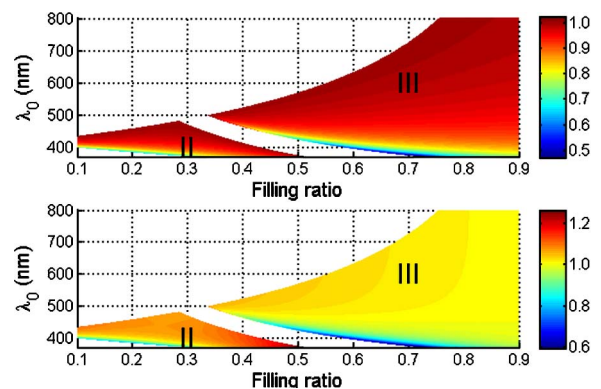


Fig. 3. (Color online) SM wavelengths on an air–metamaterial interface versus free-space wavelengths and filling ratios: (a) normalized to λ_0 and (b) normalized to the wavelengths of the SMs on an air–Ag interface λ_{Ag} .

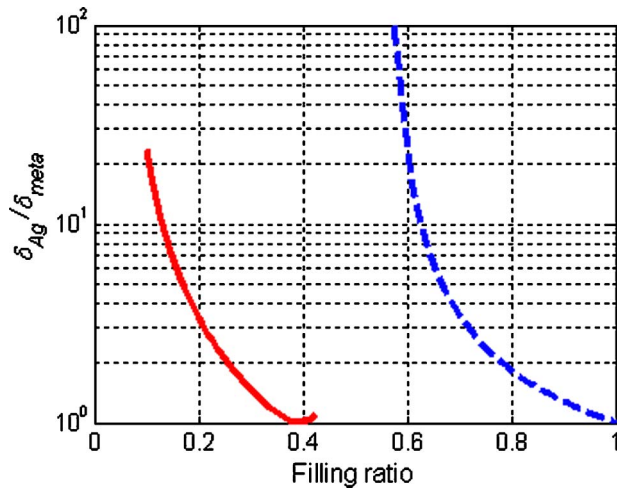


Fig. 4. (Color online) Normalized propagation length $\delta_{Ag}/\delta_{meta}$ as a function of the filling ratio for $\lambda_0 = 400$ nm: solid curve, quadrant II; dashed curve, quadrant III.

varying the metal filling ratio linearly from 0.6 to 0.9, from the center to the edge of the lens in the radial direction. It is important to emphasize that the linear profile in the filling ratio is for demonstration purposes, and it can yet be optimized to reduce the losses produced by scattering, which can be done by engineering the effective modal index in the radial direction [19]. If this step is done properly, a stronger focus can be achieved. A high filling ratio at the edge is to reduce the surface wave propagation loss, and a low filling ratio at the center is to achieve high k vectors and thus a smaller focal spot size. The thickness (in the z direction) of the lens is 150 nm. As is ana-

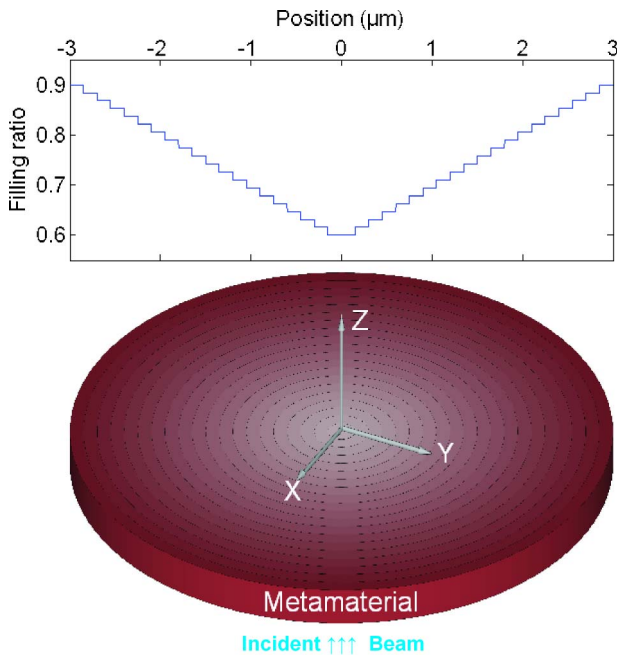


Fig. 5. (Color online) Schematic of the inhomogeneous metamaterial SM lens. The lens was designed by use of 20 coaxial cylinders, each of which has different effective permittivities that are determined by its metal filling ratio.

lyzed above, the use of inhomogeneous metamaterials can serve to mitigate the high loss problem, because the surface wave will propagate only a small distance through a medium with high losses. As a result, a focus can be formed at the center of the lens where a high k vector is supported. The metamaterial with a linear inhomogeneous profile serves as a specific example but could be adapted to any space-variant inhomogeneous profiles for further optimization purposes.

To demonstrate the proposed design, we carried out numerical simulations using Microwave Studio (Computer Simulation Technology, Framingham, Massachusetts), which calculates the electromagnetic response of metallic and dielectric objects with the finite difference time domain (FDTD) method. The coordinate system in the simulations is shown in Fig. 5. In all cases the incident electromagnetic wave propagates along the z axis and is polarized in the x axis. To simulate the materials with an anisotropic permittivity, the Drude model is used to fit the permittivity in each direction.

Figure 6 shows the simulation results of the proposed metamaterial surface wave lens and the 150 nm thick Ag plasmonic lens at the same wavelength of 400 nm. The results were plotted at the plane that is 10 nm above the lens surface. Figures 6(a) and 6(b) compare the $|E_x|^2$ profiles of the metamaterial lens and the Ag lens. It can be seen that a smaller focus of 84 nm is achieved with the metamaterial lens, in comparison with the focus of 102 nm obtained with the pure Ag plasmonic lens. Figures 6(c) and 6(d) show the comparison of $|E_z|^2$ profiles in both lenses. There is a node at the center of the $|E_z|^2$ profiles instead of a maximum as in the $|E_x|^2$ profiles [4,24]. In general, the E_z component is stronger than the E_x component. Therefore, the total intensity will present a node instead of a maximum in the plasmonic lens and in the inhomogeneous

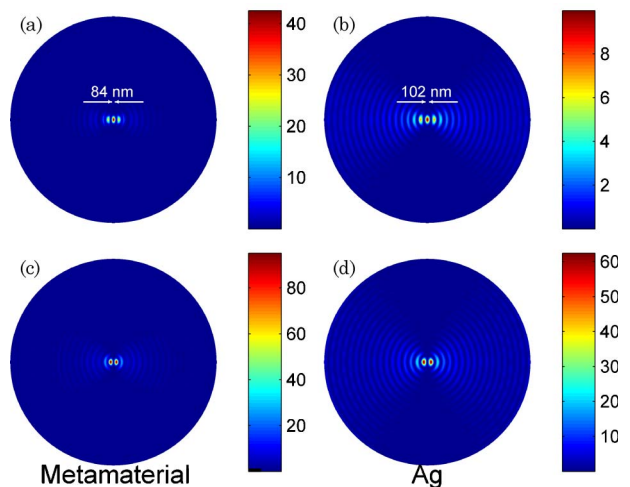


Fig. 6. (Color online) (a),(c) $|E_x|^2$ and $|E_z|^2$ of the metamaterial surface wave lens; (b),(d) $|E_x|^2$ and $|E_z|^2$ of a Ag plasmonic lens. The polarization of the excitation light is along the horizontal direction (x axis).

metamaterial lens [4]. A maximum at the center of the total intensity profile can be achieved using radially polarized light, which would also provide a stronger coupling of light into the SM and thus enhancement of the field at the focus [25].

5. Conclusions

We have proposed a new type of surface wave focusing lens using inhomogeneous metamaterials. In comparison with a pure Ag plasmonic lens, the use of inhomogeneous metamaterials presents the advantage to achieve smaller focal spots. The metamaterial is made inhomogeneous by varying the filling ratio of metal along the radial direction of the lens, thus decreasing the propagation distance of the surface waves on the high loss mematerial. With our metamaterial lens we achieved a focal spot of 84 nm, which is approximately $\lambda_0/5$ at the wavelength of 400 nm.

The authors thank R. Aguinado for fruitful discussions.

References

1. W. L. Barnes, A. Dereux, and T. W. Ebbesen, "Surface plasmon subwavelength optics," *Nature* **424**, 824–830 (2003).
2. E. Ozbay, "Plasmonics: merging photonics and electronics at nanoscale dimensions," *Science* **311**, 189–193 (2006).
3. K. A. Willets and R. P. Van Duyne, "Localized surface plasmon resonance spectroscopy and sensing," *Annu. Rev. Phys. Chem.* **58**, 267–297 (2007).
4. Z.-W. Liu, Q.-H. Wei, and X. Zhang, "Surface plasmon interference nanolithography," *Nano. Lett.* **5**, 957–961 (2005).
5. A. P. Hibbins, B. R. Evans, and J. R. Sambles, "Experimental verification of designer surface plasmons," *Science* **308**, 670–672 (2005).
6. J. B. Pendry, L. Martin-Moreno, and F. J. Garcia-Vidal, "Mimicking surface plasmons with structured surfaces," *Science* **305**, 847–848 (2004).
7. H. Ditlbacher, J. R. Krenn, G. Schider, A. Leitner, and F. R. Aussenegg, "Two-dimensional optics with surface plasmon polaritons," *Appl. Phys. Lett.* **81**, 1762–1764 (2002).
8. Z. Liu, Y. Wang, J. Yao, H. Lee, W. Srituravanich, and X. Zhang, "Broad band two-dimensional manipulation of surface plasmons," *Nano. Lett.* **9**, 462–466 (2009).
9. L. Yin, V. K. Vlasko-Vlasov, J. Pearson, J. M. Hiller, J. Hua, U. Welp, D. E. Brown, and C. W. Kimball, "Subwavelength focusing and guiding of surface plasmons," *Nano. Lett.* **5**, 1399–1402 (2005).
10. M. I. Stockman, "Nanofocusing of optical energy in tapered plasmonic waveguides," *Phys. Rev. Lett.* **93**, 137404 (2004).
11. H. Choi, D. F. Pile, S. Nam, G. Bartal, and X. Zhang, "Compressing surface plasmons for nano-scale optical focusing," *Opt. Express* **17**, 7519–7524 (2009).
12. Z. Liu, J. M. Steele, W. Srituravanich, Y. Pikus, C. Sun, and X. Zhang, "Focusing surface plasmons with a plasmonic lens," *Nano. Lett.* **5**, 1726–1729 (2005).
13. L. Salomon, G. Bassou, H. Aourag, J. P. Dufour, F. de Fornel, F. Carcenac, and A. V. Zayats, "Local excitation of surface plasmon polaritons at discontinuities of a metal film: theoretical analysis and optical near-field measurements," *Phys. Rev. B* **65**, 125409 (2002).
14. H. Raether, *Surface Plasmons on Smooth and Rough Surfaces and on Gratings* (Springer, 1988).
15. Z. Liu, J. M. Steele, H. Lee, and X. Zhang, "Tuning the focus of a plasmonic lens by the incident angle," *Appl. Phys. Lett.* **88**, 171108 (2006).
16. J. M. Steele, Z. Liu, Y. Wang, and X. Zhang, "Resonant and non-resonant generation and focusing of surface plasmons with circular gratings," *Opt. Express* **14**, 5664–5670 (2006).
17. W. Yan, L. Shen, L. Ran, and J. A. Kong, "Surface modes at the interfaces between isotropic media and indefinite media," *J. Opt. Soc. Am. A* **24**, 530–535 (2007).
18. D. R. Smith and D. Schurig, "Electromagnetic wave propagation in media with indefinite permittivity and permeability tensors," *Phys. Rev. Lett.* **90**, 077405 (2003).
19. J. Elser, R. Wangberg, V. A. Podolskiy, and E. E. Narimanov, "Nanowire metamaterials with extreme optical anisotropy," *Appl. Phys. Lett.* **89**, 261102 (2006).
20. W. Lee, R. Ji, U. Gösele, and K. Nielsch, "Fast fabrication of long-range ordered porous alumina membranes by hard anodization," *Nat. Mater.* **5**, 741–747 (2006).
21. H. Masuda and K. Fukuda, "Ordered metal nanohole arrays made by a two-step replication of honeycomb structures of anodic alumina," *Science* **268**, 1466–1468 (1995).
22. T. Thurn-Albrecht, J. Schotter, G. A. Kastle, N. Emley, T. Shibauchi, L. Krusin-Elbaum, K. Guarini, C. T. Black, M. T. Tuominen, and T. P. Russell, "Ultra-high-density nanowire arrays grown in self-assembled diblock copolymer templates," *Science* **290**, 2126–2129 (2000).
23. Y. Liu, G. Bartal, and X. Zhang, "All-angle negative refraction and imaging in a bulk medium made of metallic nanowires in the visible region," *Opt. Express* **16**, 15439–15448 (2008).
24. H. Kim and B. Lee, "Diffractive slit patterns for focusing surface plasmon polaritons," *Opt. Express* **16**, 8969–8980 (2008).
25. G. M. Lerman, A. Yanai, and U. Levy, "Demonstration of nanofocusing by the use of plasmonic lens illuminated with radially polarized light," *Nano. Lett.* **9**, 2139–2143 (2009).